THE JOURNAL OF PHYSICAL CHEMISTRY B

Article

pubs.acs.org/JPCB

Shear Thinning Three-Dimensional Colloidal Assemblies of Chitosan and Poly(lactic acid) Nanoparticles

Rémi Roux, Catherine Ladavière, Alexandra Montembault, Laurent David, and Thierry Delair*

IMP@LYON1, UMR CNRS 5223, Université de Lyon, Université Lyon 1, 15 bld Latarjet, 69622, Villeurbanne Cedex, France

Supporting Information

ABSTRACT: In this study, new materials capable of reversible self-assembly, based on concentrated negatively charged poly(lactic acid) nanoparticles and chitosan, a natural polycationic polymer, were successfully fabricated. Electrostatic interactions between oppositely charged components along with weaker interactions led to the formation of a 3D network. The resulting macroscopic assemblies were characterized by dynamic mechanical measurements, and the influences of various parameters such as chitosan/poly(lactic acid) weight ratio, duration and temperature of the mixture, and molecular weight or chitosan degree of acetylation were studied. Our results showed that the mechanical properties of assemblies were highly dependent on the nanoparticle solid content and chitosan/nanoparticle ratio. In particular, at an optimum weight ratio the colloidal assemblies exhibited remarkable high elastic moduli (about 300 kPa) for a particle solid content of 18% w/w. Thanks to the weak and reversible nature of the interactions, these materials exhibited shear thinning properties, and could instantly recover their cohesiveness at rest. The mode of interactions between PLA particles and chitosan was shown to be in part due to electrostatic interactions, but the cross-linking of chitosan-covered particles was attributed to hydrogen bonding. These materials could be envisaged as good candidates for injectable scaffolds for tissue engineering, taking advantage of the biocompatibility and bioactivity of both components. However, some issues concerning temperature stability must be resolved before applying these colloidal assemblies to cell growth in physiological conditions.

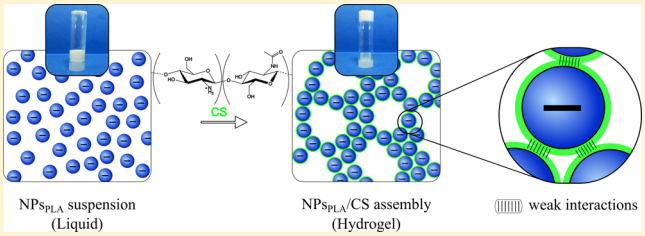

1. INTRODUCTION

The field of tissue engineering has intensively developed over these past years to meet the tremendous need in skin,[1] organ, and orthopedic surgery.[2−4] It demands the elaboration of functional three-dimensional (3D) tissue using cells combined with scaffolds featuring desired mechanical properties,[5] to favor cell growth, organization, and differentiation. Injectable scaffolds hold great promise because they can be introduced under liquid form, thus facilitating surgery, diminishing cost and delay, and improving the patient's comfort.[4,6,7] Designing such materials is a challenge as they should be liquid during the injection, and the network should form spontaneously in situ once deposited, to perfectly fit the defect and allow cell growth.

Hydrogels are highly hydrated 3D networks, widely used in tissue engineering because they provide a favorable medium for cell growth and differentiation that mimics the physiological environment.[8] Research in recent years has particularly focused on in situ forming hydrogels,[4,9] as a noninvasive method, as an alternative to open surgery, and which could be loaded with various bioactive agents. To obtain injectable hydrogels, various methods were developed, by either chemical or physical cross-linking. Chemical grafting can be carried out via radical polymerization,[10] photopolymerization,[11] and sulfide or sulfate chemistry, but this strategy raises the issue of biocompatibility because of the potentially toxic residual reactive moieties.[12] Physically cross-linked hydrogels are commonly obtained from temperature or pH sensitive polymers (PEO−PPO copolymers, pNIPAm, natural polymers, etc.). The sol−gel transition relies on physical cross-linking, based on electrostatic interactions, hydrogen bonding, and van der Waals interactions. However, the mechanical properties of physical hydrogels are often limited in comparison with chemically cross-linked hydrogels.[13]

Particular attention must be paid to mechanical strength in the development of injectable scaffolds. In recent years, hydrogel composites, especially those laden with colloids, have given rise to extensive research. They feature enhanced mechanical properties compared to noncomposite hydrogels.[14] Holland et al. have shown that colloids could also enhance the biodegradability of the hydrogel, acting as good enzymatically generated porogens.[15]

Poly(lactic acid) (PLA) is a biodegradable polyester often used as a micro-/nanovector for drug delivery because of its biocompatibility and nontoxicity.[16−19] It is also commonly used as a material for the elaboration of scaffolds for tissue engineering,[20,21] and it has been approved by the U.S. Food and Drug Administration for various biomedical applications. The degradation of PLA leads to lactic acid, which is resorbed by the body. In our research group, PLA nanoparticles were

Received: February 19, 2013
Revised: May 17, 2013

 © XXXX American Chemical Society dx.doi.org/10.1021/jp4017486 | J. Phys. Chem. B XXXX, XXX, XXX−XXX

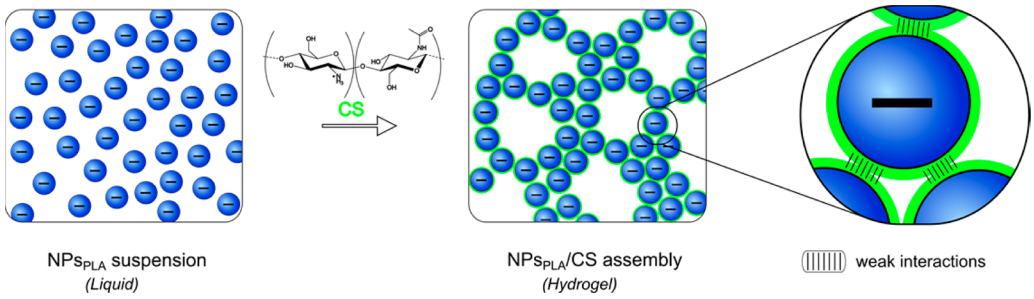

Figure 1. Complexation of negative PLA nanoparticles (NPs_{PLA}) with chitosan polycationic chains (CS) leading to a macroscopic hydrogel. CS adsorbed as a thin layer (represented in green) onto the NPs_{PLA} surface, leading to the assembly via weak interactions (black stripes).

extensively studied.[22−25] Chitosan (CS) is a cationic polysaccharide, obtained by deacetylation of chitin, one of the most abundant natural polymers. CS, a $\beta(1\rightarrow4)$-copolymer of glucosamine and *N*-acetyl-D-glucosamine, can feature positive charges along its backbone in acidic conditions, owing to the protonation of the amine moieties. CS is under intense investigation for drug delivery, gene therapy, and tissue engineering.[26] Its outstanding biological properties make it a very popular actor for repair of soft or hard tissue such as skin, cartilage, or bone.[27,28]

The aim of this work was to develop injectable, in situ forming scaffolds for tissue engineering based on one of the most widely accepted biodegradable polymers, PLA, relying on a self-assembly strategy taking place in an aqueous, tissue-friendly environment. The self-assembly process should lead to materials with high moduli after in situ incorporation, so the strategy was based on electrostatic interactions between negatively charged PLA nanoparticles (uniform size 200 nm) and positively charged chitosan (CS) (Figure 1). The adsorption of CS chains on the particle surface led to macroscopic hydrogels. These new materials were characterized by rheological and small-angle X-ray scattering (SAXS) measurements, and the influences of different parameters (inherent to CS or to environmental conditions such as temperature or mixing time) on the mechanical properties of the material were examined.

The materials reported here arose from the assembly of a polymer and a colloid but differed from most composites since the polymer matrix binding the particles remained a minor component. Hence, these materials can be regarded as a new variant of colloidal assemblies.

2. MATERIALS AND METHODS

2.1. Materials. Chitosan 114 ($\overline{M_w}$ ~ 400 kg/mol, Đ = 1.7, DA = 3%) was provided by Mahtani Chitosan (Veraval, Gujarat, India). Acetic acid, (≥99.8%), ammonium acetate (≥97%), and deuterated dimethyl sulfoxide (DMSO-d_6, >99.8%) were obtained from Carlo Erba (Val de Reuil, France). Acetone (≥99%), ethanol (96% v/v), acetic anhydride (≥99%), methyl cellulose (MeCell, powder, viscosity 4000 cP, 2% in water at 20 °C, $\overline{M_w}$ = 350 kg/mol determined in our laboratory), and deuterium oxide (D_2O, >99%), were provided by Sigma-Aldrich (Saint Quentin Fallavier, France). Poly(D,L-lactic acid) (PLA, $\overline{M_w}$ = 49 kg/mol, Đ = 1.7) with a carboxylic acid end group was obtained from Phusis (Saint Ismier, France).

2.2. Preparation and Characterization of Chitosan. To obtain high-purity chitosan, the polymer was successively solubilized at 0.5% (w/w) in a 50 mM acetic acid solution, filtered through membranes (Millipore) with a decreasing pore size from 3 to 0.45 μm, precipitated with dilute ammonium hydroxide, extensively rinsed with deionized water until neutral pH, and finally freeze-dried.

Purified chitosan was N-acetylated with acetic anhydride in homogeneous medium to obtain polymers with different degrees of acetylation (DA). The reaction was performed in a hydroalcoholic medium (water−propanediol), according to the method described by Vachoud et al.[29] After reaction, chitosans were neutralized with dilute ammonium hydroxide, rinsed with deionized water, and then freeze-dried.

The low molecular weight chitosan was produced by a nitrous deamination reaction.[30,31] Chitosan was dissolved at 0.5% (w/v) in a 0.2 M acetic acid/0.15 M ammonium acetate buffer (pH 4.5). Then, a 0.12 M sodium nitrite solution was added to the solution to obtain a molar nitrite/glucosamine ratio of 0.19. The reaction was performed under moderate magnetic stirring for 90 min. The reaction was then quenched by adding dilute ammonium hydroxide. After several washings with deionized water until neutrality, low molecular weight chitosans were freeze-dried.

The DA of chitosan was determined by ^{1}H NMR spectroscopy (Varian, 500 MHz), according to the method developed by Hirai et al.[32] The DA of chitosans was not altered by the depolymerization reaction as similar DA values were obtained before and after the hydrolysis. ^{1}H NMR analyses also allow us to check the absence of propanediol within the acetylated chitosans. The water content was determined by thermogravimetric analysis (DuPont Instrument 2950). The weight-average molecular weight ($\overline{M_w}$) and the molar-mass dispersity (Đ) were measured by gel permeation chromatography (2500 and 6000 TSK PW gel columns, i.d. = 7.8 mm and L = 300 mm) coupled online with a differential refractometer (Optilab T-rEX, Wyatt Technology) and a multiangle laser light scattering (MALLS) instrument (Dawn EOS, Wyatt Technology) equipped with a laser operating at λ = 690 nm. A degassed and filtered (on 0.1 μm membrane) 0.2 M acetic acid/0.15 M ammonium acetate buffer (pH 4.5) was used as eluent. This buffer was also used as a solvent for samples, and the resulting solutions were filtered on a 0.45 μm membrane before injection. Light intensity measurements were achieved considering a chitosan DA-dependent refractive index increment (dn/dc) according to Schatz et al.[33] The dn/dc value used for MeCell was 0.131 mL/g, and it was measured with the same differential refractometer as above.

The molecular features of chitosan samples used in this work are presented in Table 1.

2.3. Preparation and Characterization of PLA Nanoparticles. Surfactant-free PLA nanoparticles (NPs_{PLA}) were

dx.doi.org/10.1021/jp4017486 | J. Phys. Chem. B XXXX, XXX, XXX−XXX

Table 1. Characteristics of PLA Nanoparticles and Chitosan Used in this Study

PLA Nanoparticles			
sample	Z-av diam[a] (nm)	PdI[a]	ζ potential[a] (mV)
NPs_{PLA}	203	0.01	−30
Chitosans			
sample	$\overline{M_w}$[b] (10 kg/mol)	Đ[b]	DA[c] (%)
CS400DA03	400	1.7	3
CS450DA30	450	1.7	28
CS450DA55	450	1.7	55
CS20DA03	20	1.4	3

[a]Determined by quasi-elastic light scattering analyses. [b]Measured from MALLS/refractive index (RI)/size exclusion chromatographic (SEC) analyses. [c]Determined by ^{1}H NMR spectroscopy.

prepared using the nanoprecipitation method initially described by Fessi et al.[34] Briefly, the polymer was dissolved at a concentration of 2% w/v in acetone, and the mixture was slowly added to a hydroalcoholic solution under moderate stirring. The mass transfer of acetone into the continuous water phase led to the formation of NPs_{PLA}. After completion, the solvents were removed by evaporation under reduced pressure at 30 °C until the desired volume was reached. A dispersion of NPs_{PLA} with a maximum solid content of 18.8% was obtained, and further concentrations were prepared through dilutions with sterile water (pyrogen-free).

The solid content of the dispersion was measured by thermogravimetric analysis (DuPont Instrument 2950). The NPs_{PLA} size and size distribution were determined by quasi-elastic light scattering at 25 °C, at an angle of 173°, using a Zetasizer Nano ZS (Malvern Instruments Ltd., Worcestershire, U.K.), equipped with a 4 mW He/Ne laser beam operating at 633 nm. Data were analyzed using the cumulant method.[35] The polydispersity value (PdI) measured is a dimensionless parameter defined as the ratio μ_2/Γ^2, where μ_2 is the second cumulant of the correlation function and Γ is the average decay rate. Each value was the average of three series of 10 measurements. Characteristics of synthesized NPs_{PLA} are reported in Table 1.

2.4. Preparation of Colloidal Assemblies. Chitosan solutions were prepared at solid contents between 0.10 and 2% by solubilizing appropriate weights of lyophilized polymer (taking into account the water content) and adding acetic acid in stoichiometry with respect to the free amines for each chosen DA. Weighted amounts of chitosan solution and NPs_{PLA} dispersion were mixed together to obtain a final blend of known chitosan and PLA solid contents, respectively $\%^f_{CS}$ and $\%^f_{PLA}$ (expressed as w/w), deducted from initial concentrations of the two components.

2.5. Rheological Characterization. Dynamic rheological measurements were performed with a controlled stress rheometer (ARES, TA Instruments), using homemade mechanically roughened (to avoid wall slip) parallel plates of

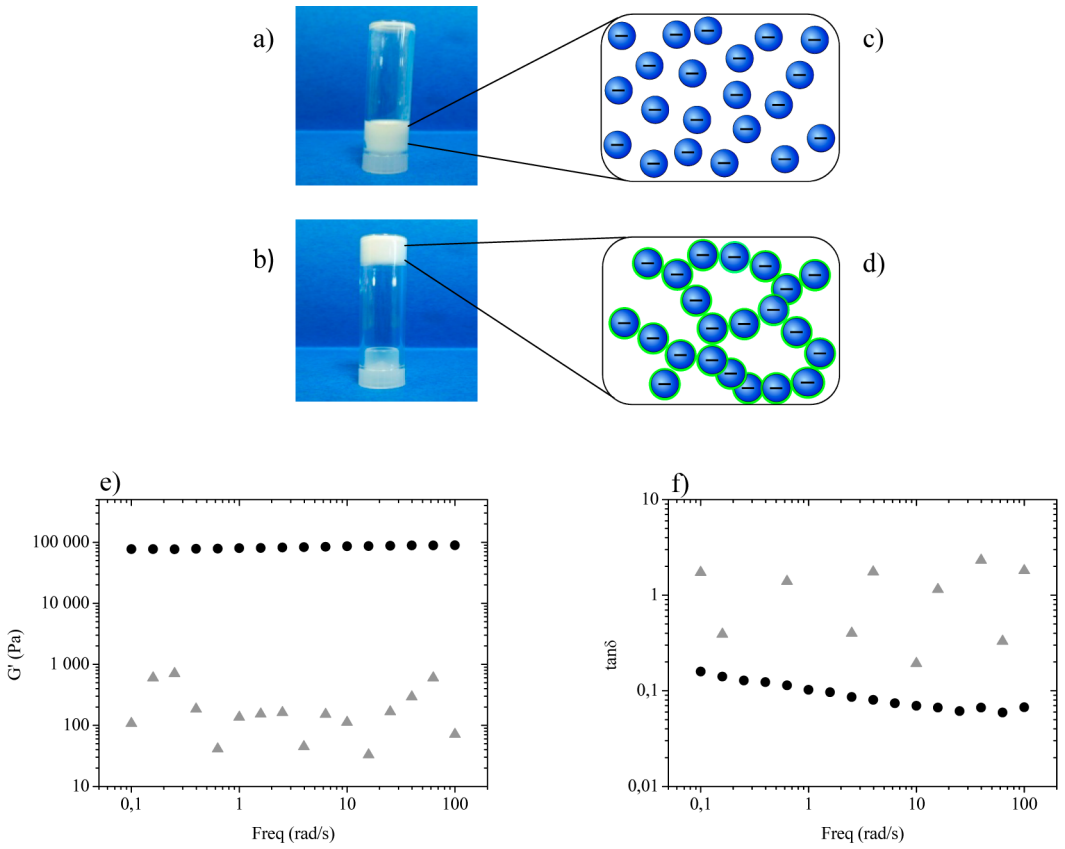

Figure 2. Formation of the NPs_{PLA}/CS400 assembly ($\%^f_{PLA}$ = 18% and $\%^f_{CS}$ = 0.033%). Tube inversion tests for NPs_{PLA} dispersion alone (a) and for colloidal assembly (b), 5 min after inversion. (c) Schematic representation of the NPs_{PLA} free in dispersion alone versus (d) the chitosan-cross-linked NPs_{PLA} assembly. Evolution of (e) G' and (f) tan δ during frequency sweep of NPs_{PLA} dispersion alone (gray triangles) and colloidal assembly (black circles). The dispersion alone had a liquidlike behavior ($G' \sim 100$ Pa and tan $\delta > 1$), while adding chitosan linked together the nanoparticles and afforded a gel behavior ($G' \sim 100$ kPa, independent of frequency, and tan $\delta < 0.1$).

dx.doi.org/10.1021/jp4017486 | J. Phys. Chem. B XXXX, XXX, XXX−XXX

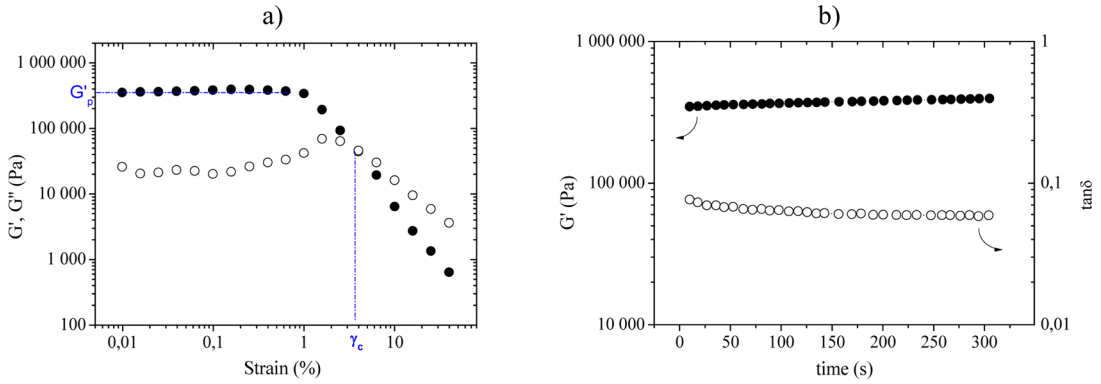

Figure 3. Shear thinning properties of NPs_{PLA}/CS400 assemblies. A sample with $\%^{f}_{PLA}$ = 18% and $\%^{f}_{CS}$ = 0.033% formed immediately a gel after mixing of the two components, with tan $\delta \sim 0.1$ ($G' \sim 10\ G''$) at low strain, in (a) strain sweep measurements, and flowed above a critical strain γ_c, defined as the strain when G' and G'' overcross. The gel recovered its cohesiveness immediately after, as seen in time sweep measurements (b).

8 mm. Immediately after preparation, samples were placed between the plates with a gap varying from 1 to 1.5 mm, depending on the samples.

We studied the evolution of G' and G'', respectively shear storage modulus and shear loss modulus, through strain sweep measurements, with an increasing oscillatory strain (from 0.05 to 50%) in a logarithmic ramp profile, while frequency was kept constant (ω = 5 rad/s). Frequency sweep tests from 100 to 0.1 rad/s were also carried out on specified samples at a strain of 0.2% located within the linear viscoelastic regime.

2.6. Synchrotron SAXS Measurements. Small-angle X-ray scattering (SAXS) measurements were performed at the BM2-D2AM beamline (ESRF, Grenoble, France). A monochromatic beam at incident energy of 16 keV was used in our study in order to characterize suspensions placed within silica glass tubes of 2 mm internal diameter (Deutero GMBH). The size of the beam was about 250 μm width and 100 μm height. The sample−detector distance was about 1.5 m. The intensity scattered by the empty cell (empty tube filled with solvent only) was subtracted from all the samples. An X-ray CCD camera from Ropper Scientific was used. Data analyses were performed with OriginPro 8.5 software. The data correction consisted of a subtraction of the dark image (image obtained with no incident beam but with the same exposure and reading conditions), normalization by the flat field (response of the camera to a homogeneous incident flux), correction by the camera distortion, and finally a normalization by the transmitted intensity that yielded corrected images that were further used to produce radial averages around the image center (beam center). The normalization of the image with transmitted intensity was also performed. The scattering vector range was calibrated thanks to silver behenate.

3. RESULTS AND DISCUSSION

3.1. Description of the NP_{PLA}/CS Gel Formation. Zeta (ζ) potential measurements indicated that PLA nanoparticles carried negative charges on their surface (ζ = −30 mV, Table 1), conferred by carboxylic acid end groups. NPs_{PLA} benefited from an efficient electrostatic repulsion, and the colloidal dispersion had a high stability and a very low viscosity, close to water, even at high solid content. This naked eye observation (see tube inversion test in Figure 2a) was confirmed by frequency sweep measurements, where the G' modulus of the 18.8% w/w dispersion (the maximum tested solid content here) was very low (gray triangles in Figure 2e), close to the detection limit of the rheometer.

When acidic solutions of chitosan were added to the NPs_{PLA} dispersion, gelation occurred instantly (see Figure 2b) and the G' modulus increased significantly (black circles in Figure 2e). The tan δ (defined as G''/G') also strongly decreased to reach ca. 0.1 and stabilized below 0.1 (see Figure 2f), over several frequency decades, suggesting that the system was mainly elastic and had a gel behavior. To check that the assembly was indeed initiated by the cationic polysaccharide, we ran blank experiments substituting chitosan with acidic water (containing the same amount of acetic acid used to dissolve chitosan) or protonated glucosamine, the main repeat unit of chitosan, in water at the same concentration as for chitosan. Under all these conditions no gelation was observed (results not shown). In acidic conditions, amine moieties of chitosan are protonated, and the polymer provided many positive charges along the backbone, especially since its DA was very low. When mixed together, for appropriate weight ratios, positively charged chains of chitosan and negatively charged NPs_{PLA} self-assembled (see Figure 1), leading to a macroscopic gel.

It is worth noting that the acid amount in the composite assemblies is very low (see Table S1 in the Supporting Information) and is used to obtain chitosan acetate. Though CS has been successfully used in various tissue engineering applications,[26−28] the impact of acidity on cytocompatibility will need to be assessed in further investigations.

3.2. Shear Thinning Properties and Gel Recovery. An important aspect of scaffold development for tissue engineering is the possibility of injecting the material with a subsequent in situ gelation, thus easing the implantation protocol. Our NPs_{PLA}/CS assemblies exhibited shear thinning properties, and shear sweep measurements highlighted this phenomenon. The general behavior of such assemblies under stress is presented in Figure 3: at low strain values, both G' and G'' remained constant with a plateau value for G' called here G'_p, and tan $\delta <$ 0.1 (see Figure 3a), indicating that the assembly behaved like a viscoelastic gel. As γ increased, G' started to decrease while G'' passed through a maximum before decreasing as well. Such a G'' peak was observed in other works and could be related to a highly dissipative process going on in the network microstructure.[36−38] After this G'' peak, both moduli crossed over and then decreased with a power law (with G'' always above G'). This behavior can be described by the disruption of the gel network as the physical cross-links of colloidal assemblies relied

dx.doi.org/10.1021/jp4017486 | J. Phys. Chem. B XXXX, XXX, XXX−XXX

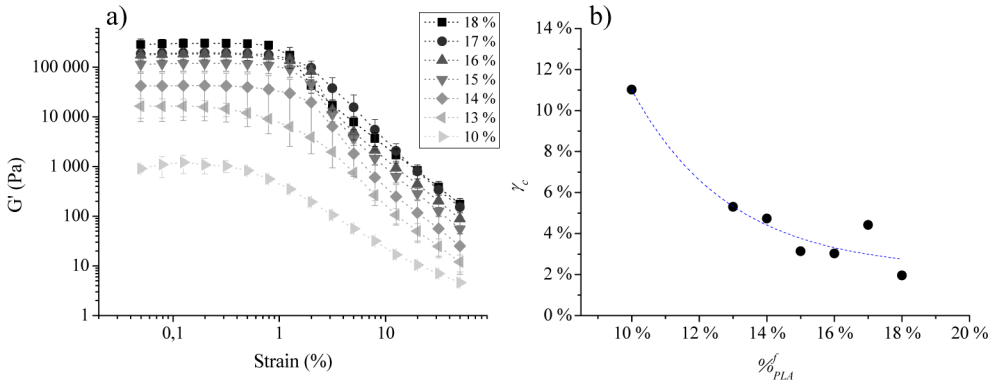

Figure 4. Influence of $\%^f_{PLA}$ on the rheological behavior of NPs_{PLA}/NPs_C assemblies. (a) Dynamic strain sweep measurements on different samples with CS400 ($\%^f_{CS}$ kept constant at 0.033%) as a function of $\%^f_{PLA}$; (b) corresponding γ_c plotted versus $\%^f_{PLA}$.

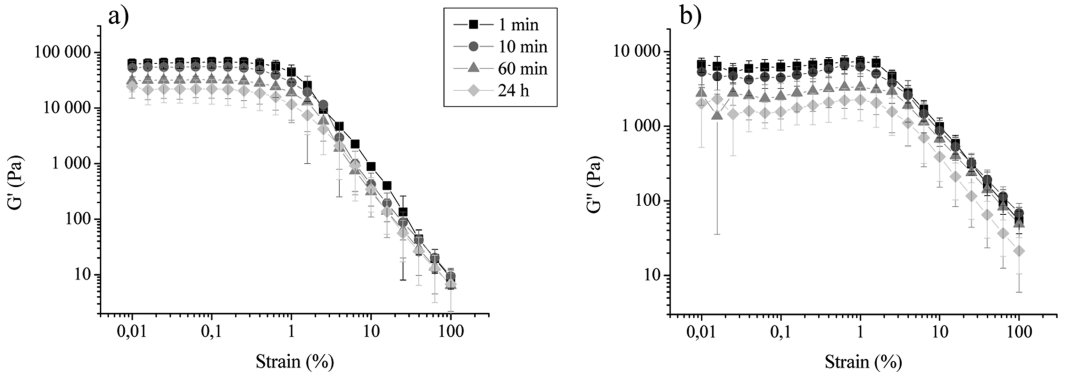

Figure 5. Dynamic strain sweep measurements ((a) G' and (b) G'') as a function of storing time of NPs_{PLA}/CS400 assembly ($\%^f_{PLA}$ = 17%; $\%^f_{CS}$ = 0.024%). For readability reasons, some G' error bars of assemblies 1 and 10 min at high strains have been hidden.

on a combination of electrostatic interactions between positive charges along chitosan chains and the negative charges onto the NPs_{PLA} surface, and weak interactions between CS-covered particles (see discussion in section 3.5). The G' and G'' crossover is commonly defined as the critical yield strain, denoted here as γ_c (see Figure 3a), and corresponds to the strain required to turn the gel to a fluid.[39,40]

Once strain sweep tests were done, time sweep tests were immediately launched on the same sample, with a fixed frequency and strain of 5 rad/s and 0.2%, respectively, to evaluate the recovery of mechanical properties. As reported in Figure 3b, the cohesiveness of the NPs_{PLA}/CS assembly was immediately restored since the G' modulus reached from the first seconds the same value as the G'_p, and tan δ was below 0.1. These results indicate that the system recovered immediately its cohesiveness and gel behavior, which is a major advantage for in situ gelling applications.

3.3. Influence of the PLA Concentration. The mechanical properties of NPs_{PLA}/CS assemblies were directly impacted by the PLA content. Dynamic strain sweep tests on samples prepared with constant CS400 concentration ($\%^f_{CS}$ = 0.033%) and PLA concentration ($\%^f_{PLA}$) ranging between 10 and 18% w/w were carried out, and results are presented in Figure 4. G'_p increased with $\%^f_{PLA}$, reaching a maximum of about 300 kPa for the highest solid content. This result is not surprising since an increase in particle content led to a decrease in the interparticular distance, thus promoting particle−particle interactions and increasing the elastic behavior.[41] Interestingly, the PLA content also impacted γ_c (see Figure 4b), which decreased with increasing $\%^f_{PLA}$, as observed in a previous study[41] for concentrated silica colloids.

3.4. Time and Temperature Dependence. The rheological behavior of NPs_{PLA}/CS assemblies was investigated with time, and Figure 5 presents the results of strain sweep measurements on NPs_{PLA}/CS400 ($\%^f_{PLA}$ = 17% and $\%^f_{CS}$ = 0.024%) performed at four different times (immediately after mixing, 10 min after, 60 min after, and 24 h after), with each curve being the average of three independent experiments. Each sample was sealed during the storage period to prevent water evaporation. Despite a high standard deviation, the observed trend was a decrease of G'_p with time: the initial value after mixing of 67 kPa reached 22 kPa after 24 h. This can be explained by a reorganization of chitosan chains decreasing the number of weak interactions between CS-covered particles, or by a time-dependent ordering of NPs_{PLA}/CS leading to the formation of larger aggregates thus decreasing the density of cross-links and consequently the mechanical properties of the assemblies.

To investigate the possible influence of temperature on the behavior of NPs_{PLA}/CS assemblies, we prepared at room temperature 3 × 3 samples (with $\%^f_{CS}$ = 0.024% and $\%^f_{PLA}$ = 17%), which were stored for 24 h at 4, 22, and 37 °C. Each sample was sealed to prevent water evaporation. After this treatment, the rheological behavior of the gels was examined by strain sweep measurements. The plateau modulus increased with decreasing temperature from 22 °C (G'_p = 10 ± 1.5 kPa) to 4 °C (G'_p = 53 ± 20 kPa). It is known that a temperature decrease favors the formation of hydrogen bonds.[42,43] Hence, the increased cohesiveness of colloidal assemblies on cooling

dx.doi.org/10.1021/jp4017486 | J. Phys. Chem. B XXXX, XXX, XXX−XXX

can be attributed to the formation of interchain hydrogen bonds, known to play a major role in CS autoassociation.[44] After 24 h at 37 °C, the NPs_{PLA}/CS assemblies had shrunk and appeared as hard and brittle solids, as a high amount of water had been expelled. Because of this fragile behavior, we were not able to perform the rheological measurements. Such a behavior was unexpected at this relatively low temperature. In fact, the low molecular weight of the PLA (50 kg/mol) could be responsible for an increased sensitivity against temperature, as previously described by Omelczuk and McGinity.[45] The authors observed a decrease in T_g from 56 to 44 °C when the PLA molecular weight was decreased from 137 to 41 kg/mol. Moreover, in the presence of water, surface PLA chains may undergo plasticization, leading to an additional decrease of the T_g value. Craig et al. indeed demonstrated that the T_g of PLA could decrease from 52 to 37 °C by increasing the water content from 0 to ca. 3.5%.[46] A combination of these two phenomena could thereby lead the NPs_{PLA} to sinter irreversibly, leading to an expulsion of water and the formation of a fragile monoblock of PLA.

3.5. Influence of CS/PLA Weight Ratio (R_w). NPs_{PLA}/CS assemblies exhibiting various degrees of cohesiveness were prepared by mixing NPs_{PLA} and chitosan at different weight ratios, R_w, defined as the dry CS mass (milligrams) over the PLA mass (grams). Strain sweep measurements were conducted on these samples, and results of the plateau modulus G'_p plotted versus R_w are displayed in Figure 6. As seen before,

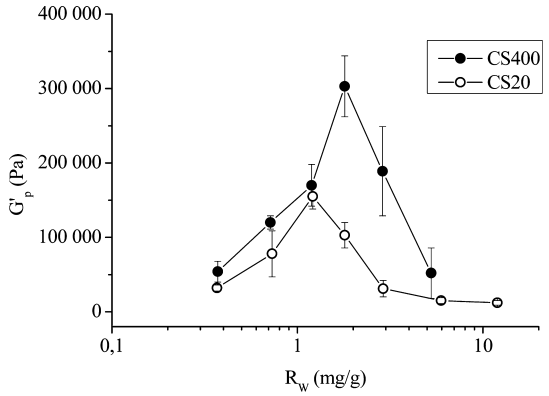

Figure 6. Evolution of plateau modulus G'_p versus mass ratio R_w. Plateau moduli of NPs_{PLA}/CS assembly based on CS400 (filled circles) and CS20 (open circles) as a function of R_w. $\%^f_{PLA}$ = 18%; $\%^f_{CS}$ varied between 0.0066 and 0.1%, for NPs_{PLA}/CS400 assemblies, and between 0.0066 and 0.2% for NPs_{PLA}/CS20 assemblies.

for NPs_{PLA} dispersion only (i.e., R_w = 0, Figure 2), the G' value was very low (close to 100 Pa) and tan δ was close to 1, corresponding to a liquidlike behavior. Increasing the chitosan content in the mixtures led to more cohesive gels, as shown by an increase in G'_p values. When R_w increased, the elastic modulus reached a maximum of ca. 300 kPa for a R_w value of 1.8 mg/g, a result in accordance with the expected increase in the density of cross-links resulting from the addition of more polycationic chains to the negatively charged nanoparticles.

When R_w was increased above 1.8 mg/g (for NPs_{PLA}/CS400), the cohesiveness of the colloidal assemblies decreased sharply as shown by the drastic reduction in G'_p (but tan δ remained lower than 0.1). In fact, an optimum chitosan to NPs_{PLA} mass ratio of R_w = 1.8 mg/g was observed, at which the network cohesiveness was maximal. This result was unexpected, as we had anticipated that as more polycationic chains were added, the assemblies became more cross-linked, on the basis that the gelation resulted from electrostatic interactions between the negatively charged colloid and the positively charged polysaccharide. Hence, we must reconsider the mode of interaction between PLA particles and chitosan responsible for the formation of an elastic gel. In a previous investigation, we showed that the adsorption of chitosan onto PLA nanoparticles was spontaneous due to electrostatic interactions between both partners.[47] Therefore, we can assume that, on adding chitosan to the concentrated PLA particle dispersion, the cationic polyelectrolyte first adsorbed at the particle interface and then the chitosan-covered particles interacted with one another to yield the gel via hydrogen bonding. The two following facts could support this hypothesis: (i) first, the optimum chitosan to PLA mass ratio was obtained at R_w = 1.8 mg/g (equivalent to an amount of 0.08 mg of chitosan/m^2 of NPs_{PLA} surface, see calculation in Table S1, Supporting Information), which is consistent with the maximum covering capacity determined in the previous work cited above: 0.11 mg/m^2 for a similar system (369 kg/mol chitosan, DA 5.2%, and NPs_{PLA} of average diameter around 250 nm); (ii) second, the fact that on cooling the elasticity increased, as discussed in section 3.4, suggesting the involvement of hydrogen bonds in the gel formation process. The decrease in modulus as R_w increased beyond the optimum value can be understood as a "plasticization" effect of unbound chitosan chains, favoring the movement of chitosan-covered PLA particles, hence the decrease in cohesiveness.

3.6. Influence of Chitosan Molecular Weight. Nitrous depolymerization provided a low molecular weight chitosan sample, with a $\overline{M}_w$ of 20 kg/mol (CS20), determined by SEC. Mixing CS20 with NPs_{PLA} dispersion also yielded hydrogels showing a shear thinning behavior. We studied the effect of R_w on NPs_{PLA}/CS20 assemblies with strain sweep test while keeping $\%^f_{PLA}$ constant (18%). As shown in Figure 6 (open circles), CS20-based gels behaved similarly to those obtained with CS400, reaching a G'_p maximum for an optimal R_w. However, G'_p values for the NPs_{PLA}/CS20 assemblies were always lower than those for the NPs_{PLA}/CS400 assemblies, with a maximum at 150 kPa (300 kPa for NPs_{PLA}/CS400), meaning that the 20 kg/mol chitosan led to assemblies of lower cohesiveness. Interestingly, the maximum G'_p was reached at R_w close to 1 mg/g, lower than for CS400, suggesting that less chitosan was necessary to achieve the surface saturation. This is in complete agreement with Messai et al., who showed that reducing the molecular weight of chitosan led to a decrease of the adsorbed amount,[47] under a rodlike conformation.[48] An increase in molar mass of chitosan resulted in a increase in chain flexibility,[49] and as described by Guo et al., some segments of the polymer chains adsorbed on the particle surface ("trains") and others formed loops extended toward the continuous phase.[50] These loops, interacting with one another, could be responsible for the increase in mechanical properties observed for CS400, but as discussed below, they were not large enough to cross-link more than two particles.

3.7. Influence of the Degree of Acetylation. The influence of the molar fraction of acetylated moieties in CS copolymer (DA) was investigated, with chitosan samples CS450DA55 and CS450DA30 obtained from homogeneous reacetylation of CS400. Assemblies NPs_{PLA}/CS450DA55 and NPs_{PLA}/CS450DA30 were prepared at $\%^f_{PLA}$ = 18% and $\%^f_{CS}$ = 0.033%, similar conditions as for CS400 at optimal R_w. Strain

dx.doi.org/10.1021/jp4017486 | J. Phys. Chem. B XXXX, XXX, XXX−XXX

sweep tests were carried out to characterize the stiffness and compliance of the assemblies as a function of DA. Results in Figure 7 show that G'_p values for the three different assemblies

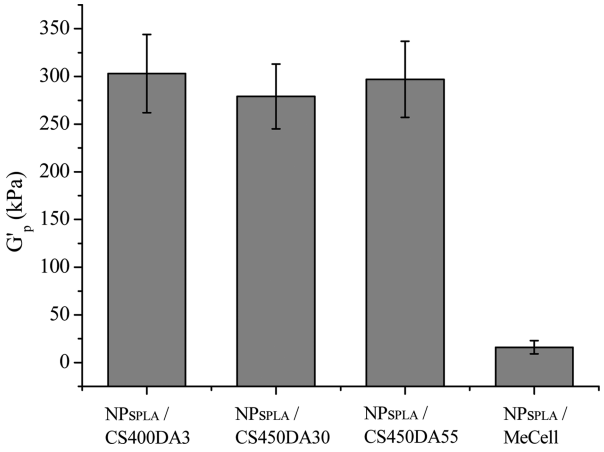

Figure 7. Influence of DA on G'_p of NPs_{PLA}/CS assemblies (R_w of all samples is equal to 0.18%). Results are the average of three independent measurements.

were similar, taking into account the standard deviation. Therefore, DA, or in other words the charge density of chitosan, had no influence on the mechanical properties of NPs_{PLA}/CS assemblies. This is in total accordance with our proposed mode of interactions favoring hydrogen bonding rather than pure electrostatic interactions. Nevertheless, to ensure that the presence of charges on the linking polymer played a major role in the assembly process, we substituted chitosan by a neutral methyl cellulose, MeCell ($\overline{M_w}$ = 350 kg/mol determined by SEC), at an identical final concentration (0.033%). Results plotted in Figure 7 showed that the NPs_{PLA}/MeCell mixture displayed a cohesiveness far lower ($G'_p \sim 16$ kPa) than NPs_{PLA} with chitosan. Experimentally, this mixture was easily flowing when dropped on a surface, contrary to the NPs_{PLA}/CS assembly. The observed lack of cohesion with MeCell confirms the hypothesis that the assembly process relied partially on electrostatic attractive interactions between chitosan positive charges and negative charges on NPs_{PLA} surfaces. However, the absence of impact of DA on the final cohesiveness of the assemblies and the fact that the maximal elasticity was found for a weight ratio corresponding to the maximal covering of the PLA particles by chitosan support the major involvement of weak interactions, H bonds, in the mechanical properties of the assemblies.

3.8. Morphological Study of NPs_{PLA}/CS Complexes. SAXS measurements were used to analyze the surface of the NPs_{PLA} particles and confirm possible chitosan adsorption onto their surface. Four samples were analyzed (see Table 2): NPs_{PLA} mixed with chitosan CS400 (entries 2 and 4) or not (entries 1 and 3), at high concentrations (entries 1 and 2, $\%^f_{PLA}$ = 18% and $\%^f_{CS}$ = 0.032%), or at 20-fold dilution (entries 3 and 4). Figure 8a shows the scattered intensities as a function of the scattering vector $q = 4\pi \sin(\theta)/\lambda$ where 2θ is the scattering angle and λ is the incident wavelength (0.7749 Å). The size of the PLA particles was large in comparison with the assessable q-range, and the Guinier behavior[51] could not be observed. All samples presented a similar scattering pattern with an $I = I_0 q^{-\alpha}$ power law in the q-range between 8×10^{-3} and 6×10^{-2} Å^{-1} with an α exponent close to 4 (Porod's law). This scattering behavior is thus characteristic of a sharp interface between PLA particles and the continuous phase. The "polyelectrolyte peak"[52] visible in pure chitosan solution could not be evidenced in the presence of the PLA particles.

Nevertheless, we could detect significant differences in the α exponents of the samples prepared with and without chitosan, with the latter presenting α values slightly lower (both 3.96) than the former (3.99 and 4.06). Such a slight difference probably reveals the low contrast between a highly hydrated chitosan corona and the aqueous medium, compared to the contrast of NPs_{PLA}. However, the difference corresponded to a density-gradient profile at the particle interface due to the presence of chitosan. Assuming the chitosan density varies linearly beyond the particle surface, we could estimate the thickness l_i of the adsorbed layer (if l_i is small compared to the particle size) using[53]

$$I(q) = C/q^4 - B/q^2 \quad (1)$$

where C is Porod's constant and B is related to the interface thickness.

Hence the I^*q^2 vs $1/q^2$ plot (see Figure 8b) was used to deduce B and C values, respectively, from the vertical axis intercept and the slope of the fitting line, determined between $1/q^2$ values of 9600 and 2650 Å^2, for which the standard deviation was minimized. l_i is deduced from the B and C values, according to

$$l_i = \sqrt{\frac{12\pi B}{C}} \quad (2)$$

NPs_{PLA} samples without chitosan, diluted or not (entries 1 and 3 in Table 2), presented the same α exponent and similar negative B values, which is consistent with a sharp particle interface with no transition layer; accordingly, no l_i value could be calculated. On the contrary, NPs_{PLA} samples with chitosan (entries 2 and 4 in Table 2) featured a positive B value, hence allowing a calculation of l_i. Results show a diffuse organized layer of chitosan at the interface, whose width ranged from about 50 to 70 Å, hence confirming the adsorption of CS on NPs_{PLA} surfaces. Interestingly, these values are low compared to the R_g of chitosan (in the range of 50 nm[54]). This supports the

Table 2. Analyses of SAXS Data[a]

entry	sample	α	B	C	l_i (Å)
1	NPs_{PLA}	3.96 ± 0.005	−184 ± 13	1.367 ± 0.002	–
2	NPs_{PLA} + CS400	4.06 ± 0.01	141 ± 35	1.188 ± 0.007	67 ± 17
3	NPs_{PLA} dil.	3.96 ± 0.006	−190 ± 2	0.1675 ± 0.0004	–
4	NPs_{PLA} + CS400 dil.	3.99 ± 0.01	17 ± 4	0.216 ± 0.0007	54 ± 13

[a]For entry 1, $\%^f_{PLA}$ = 18% ; for entry 2, $\%^f_{PLA}$ = 18% and $\%^f_{CS}$ = 0.032% ; samples of entries 3 and 4 are 20-fold dilutions of 1 and 2, respectively. α was obtained from the slope of curves in Figure 8a ; B and C are parameters obtained from the linear regression in Figure 8b; l_i was obtained by means of eq 2. Results are given as the average ± standard deviation.

dx.doi.org/10.1021/jp4017486 | J. Phys. Chem. B XXXX, XXX, XXX−XXX

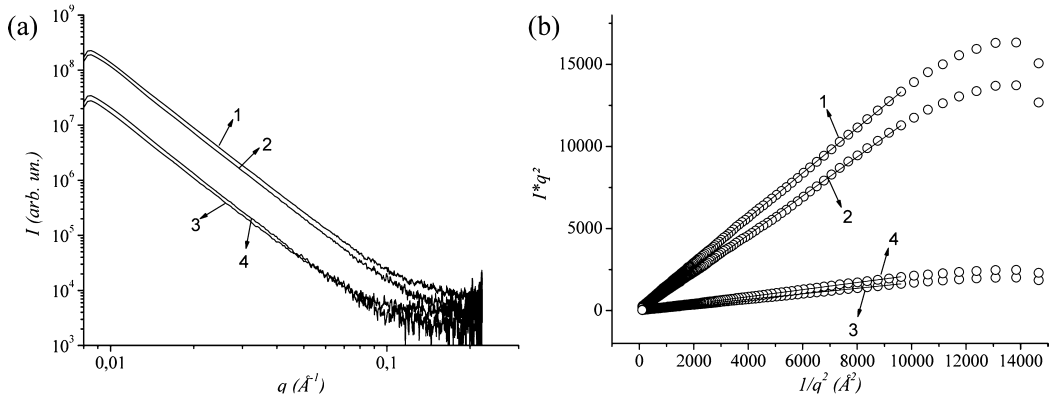

Figure 8. (a) SAXS relative intensities of different samples of NPsPLA with or without chitosan. (b) Corresponding $I*q^2$ reported as a function of $1/q^2$. Curves numbered 1−4 correspond to entries of Table 2.

"train" model of adsorption previously mentioned, with occasionally the formation of a few "loops" on the surface of the particles, too small to cross-link several particles together, but large enough to play the role of anchorage, leading to the observed increase in G'_p for NPs_{PLA}/CS400.

4. CONCLUSION

We achieved the assembly of PLA nanoparticles with chitosan, leading to a new material capable of self-gelling with shear thinning properties, based on completely biocompatible components. Upon mixing the NPs_{PLA} dispersion and the chitosan solution, a network formed instantaneously, with positively charged chitosan chains interacting with the negative surface of NPs_{PLA}. Our work established that electrostatic interactions between the particles and the polymer were necessary for the gelation to occur, but the cohesiveness of the gel was ensured by hydrogen bonding of the chitosan shell on the particles. Electrostatic attractive interactions between the colloid and the polysaccharide were involved to surface functionalize the PLA particles with an outer shell of chitosan that could cross-link via low energy interactions to achieve gelation. SAXS measurements indicated that chitosan adsorbed onto the particle surface, forming a highly hydrated layer of a few nanometers in length. Owing to this combination of low energy cross-links, the system featured shear thinning properties, essential for injections in the context of a minimally invasive therapy. The gel reformed and immediately recovered its cohesiveness, potentially favorable for reducing the delay of surgery. Mechanical properties could be tuned by varying the relative amounts of each constituent, to match the desired cohesiveness in function of the tissue to be treated. However, stability problems of PLA nanoparticles appeared, since the low molecular weight polymer used in this study proved to be very sensitive to temperature. This issue will certainly be overcome with the use of a higher molecular weight, which features an improved T_g.

This study allowed us to understand mechanisms governing the assembly of PLA particles with chitosan. To develop further this material, we will consider the stability of such systems, in cell culture conditions, which is the next step of this work. We can also plan to encapsulate or surface adsorb growth factors or other bioactive agent on the nanoparticles,[24,55] to favor cell amplification or differentiation.

■ ASSOCIATED CONTENT

Supporting Information

Details of calculations and sample preparations, and list of abbreviations. This material is available free of charge via the Internet at http://pubs.acs.org.

■ AUTHOR INFORMATION

Corresponding Author

*E-mail: thierry.delair@univ-lyon1.fr. Tel.: +33 (0)4 72 44 85 87.

Notes

The authors declare no competing financial interest.

■ ACKNOWLEDGMENTS

This work was financially supported by a grant from the French Ministry of Research and Technologies. The authors are grateful to Dr. F. Gaudin and Dr. B. Verrier (IBCP—Lyon) for PLA supplies and technical support, and Prof. R. Fulchiron and P. Cassagnau for valuable discussions concerning the rheological aspects of this work.

■ REFERENCES

(1) Metcalfe, A. D.; Ferguson, M. W. J. Tissue Engineering of Replacement Skin: The Crossroads of Biomaterials, Wound Healing, Embryonic Development, Stem Cells and Regeneration. *J. R. Soc., Interface* **2007**, *4*, 413−437.

(2) Griffith, L. G.; Naughton, G. Tissue Engineering—Current Challenges and Expanding Opportunities. *Science* **2002**, *295*, 1009−1014.

(3) Darling, E. M.; Athanasiou, K. A. Biomechanical Strategies for Articular Cartilage Regeneration. *Annu. Biomed. Eng.* **2003**, *31*, 1114−1124.

(4) Delair, T. In Situ Forming Polysaccharide-Based 3D-hydrogels for Cell Delivery in Regenerative Medicine. *Carbohydr. Polym.* **2012**, *87*, 1013−1019.

(5) Engler, A. J.; Sen, S.; Sweeney, H. L.; Discher, D. E. Matrix Elasticity Directs Stem Cell Lineage Specification. *Cell* **2006**, *126*, 677−689.

(6) Nguyen, M. K.; Lee, D. S. Injectable Biodegradable Hydrogels. *Macromol. Biosci.* **2010**, *10*, 563−579.

(7) Roux, R.; Ladavière, C.; Montembault, A.; Delair, T. Particle Assemblies: Toward New Tools for Regenerative Medicine. *Mater. Sci. Eng., C* **2013**, *33*, 997−1007.

(8) Tibbitt, M. W.; Anseth, K. S. Hydrogels as Extracellular Matrix Mimics for 3D Cell Culture. *Biotechnol. Bioeng.* **2009**, *103*, 655−663.

(9) Van Tomme, S. R.; Storm, G.; Hennink, W. E. In Situ Gelling Hydrogels for Pharmaceutical and Biomedical Applications. *Int. J. Pharm.* **2008**, *355*, 1−18.
(10) Park, H.; Temenoff, J. S.; Tabata, Y.; Caplan, A. I.; Mikos, A. G. Injectable Biodegradable Hydrogel Composites for Rabbit Marrow Mesenchymal Stem Cell and Growth Factor Delivery for Cartilage Tissue Engineering. *Biomaterials* **2007**, *28*, 3217−3227.
(11) Nguyen, K. T.; West, J. L. Photopolymerizable Hydrogels for Tissue Engineering Applications. *Biomaterials* **2002**, *23*, 4307−4314.
(12) Hou, Q.; De Bank, P. A.; Shakesheff, K. M. Injectable Scaffolds for Tissue Regeneration. *J. Mater. Chem.* **2004**, *14*, 1915−1923.
(13) Hennink, W. E.; Van Nostrum, C. F. Novel Crosslinking Methods to Design Hydrogels. *Adv. Drug Delivery Rev.* **2002**, *54*, 13−36.
(14) Arimura, H.; Ouchi, T.; Kishida, A.; Ohya, Y. Preparation of a Hyaluronic Acid Hydrogel Through Polyion Complex Formation Using Cationic Polylactide-Based Microspheres as a Biodegradable Cross-linking Agent. *J. Biomater. Sci., Polym. Ed.* **2005**, *16*, 1347−1358.
(15) Holland, T. A.; Tessmar, J. K. V; Tabata, Y.; Mikos, A. G. Transforming Growth Factor B1 Release from Oligo(poly(ethylene glycol) fumarate) Hydrogels in Conditions That Model the Cartilage Wound Healing Environment. *J. Controlled Release* **2004**, *94*, 101−114.
(16) Anderson, J. M.; Shive, M. S. Biodegradation and Biocompatibility of PLA and PLGA Microspheres. *Adv. Drug Delivery Rev.* **1997**, *28*, 5−24.
(17) Shi, X.; Wang, Y.; Varshney, R. R.; Ren, L.; Gong, Y.; Wang, D.-A. Microsphere-based Drug Releasing Scaffolds for Inducing Osteogenesis of Human Mesenchymal Stem Cells in Vitro. *Eur. J. Pharm. Sci.* **2010**, *39*, 59−67.
(18) Ignatius, A. A.; Claes, L. E. In Vitro Biocompatibility of Bioresorbable Polymers: Poly(L, DL-lactide) and Poly(L-lactide-co-glycolide). *Biomaterials* **1996**, *17*, 831−839.
(19) Biggs, D. L.; Lengsfeld, C. S.; Hybertson, B. M.; Ng, K.; Manning, M. C.; Randolph, T. W. In Vitro and in Vivo Evaluation of the Effects of PLA Microparticle Crystallinity on Cellular Response. *J. Controlled Release* **2003**, *92*, 147−161.
(20) Phattanaphibul, T.; Koomsap, P. Investigation of PLA-Based Scaffolds Fabricated via SVM Rapid Prototyping. *J. Porous Mater.* **2012**, *19*, 481−489.
(21) Serra, T.; Planell, J. A.; Navarro, M. High-resolution PLA-Based Composite Scaffolds via 3-D Printing Technology. *Acta Biomater.* **2013**, *9*, 5521−5530.
(22) Trimaille, T.; Pichot, C.; Delair, T. Surface Functionalization of Poly(d,l-lactic Acid) Nanoparticles with Poly(ethylenimine) and Plasmid DNA by the Layer-by-Layer Approach. *Colloids Surf., A* **2003**, *221*, 39−48.
(23) Taman-Onal, Y.; Munier, S.; Ganee, A.; Terrat, C.; Durand, P. Y.; Battail, N.; Martinon, F.; Le Grand, R.; Charles, M. H.; Delair, T.; Verrier, B. Surfactant-Free Anionic PLA Nanoparticles Coated with HIV-1 P24 Protein Induced Enhanced Cellular and Humoral Immune Responses in Various Animal Models. *J. Controlled Release* **2006**, *112*, 175−185.
(24) Rancan, F.; Papakostas, D.; Hadam, S.; Hackbarth, S.; Delair, T.; Primard, C.; Verrier, B.; Sterry, W.; Blume-Peytavi, U.; Vogt, A. Investigation of Polylactic Acid (PLA) Nanoparticles as Drug Delivery Systems for Local Dermatotherapy. *Pharm. Res.* **2009**, *26*, 2027−2036.
(25) Handké, N.; Trimaille, T.; Luciani, E.; Rollet, M.; Delair, T.; Verrier, B.; Bertin, D.; Gigmes, D. Elaboration of Densely Functionalized Polylactide Nanoparticles from N-Acryloxysuccinimide-Based Block Copolymers. *J. Polym. Sci., Part A: Polym. Chem.* **2011**, *49*, 1341−1350.
(26) Domard, A.; Domard, M. Chitosan: Structure-Properties Relationship and Biomedical Applications. In *Polymeric Biomaterials*, 2nd ed.; Marcel Dekker: New York, 2002; pp 187−212.
(27) Muzzarelli, R. A. A. Chitins and Chitosans for the Repair of Wounded Skin, Nerve, Cartilage and Bone. *Carbohydr. Polym.* **2009**, *76*, 167−182.
(28) Montembault, A.; Tahiri, K.; Korwin-Zmijowska, C.; Chevalier, X.; Corvol, M. T.; Domard, A. A Material Decoy of Biological Media Based on Chitosan Physical Hydrogels: Application to Cartilage Tissue Engineering. *Biochimie* **2006**, *88*, 551−564.
(29) Vachoud, L.; Zydowicz, N.; Domard, A. Formation and Characterisation of a Physical Chitin Gel. *Carbohydr. Res.* **1997**, *302*, 169−177.
(30) Allan, G. G.; Peyron, M. Molecular-Weight Manipulation of Chitosan. 1. Kinetics of Depolymerization by Nitrous-Acid. *Carbohydr. Res.* **1995**, *277*, 257−272.
(31) Allan, G. G.; Peyron, M. Molecular-Weight Manipulation of Chitosan. 2. Prediction and Control of Extent of Depolymerization by Nitrous-Acid. *Carbohydr. Res.* **1995**, *277*, 273−282.
(32) Hirai, A.; Odani, H.; Nakajima, A. Determination of Degree of Deacetylation of Chitosan by H NMR Spectroscopy. *Polym. Bull.* **1991**, *26*, 87−94.
(33) Schatz, C.; Viton, C.; Delair, T.; Pichot, C.; Domard, A. Typical Physicochemical Behaviors of Chitosan in Aqueous Solution. *Biomacromolecules* **2003**, *4*, 641−648.
(34) Fessi, H.; Devissaguet, J. P.; Puisieux, F.; Theis, C.; Thies, C. Process for the Preparation of Dispersible Colloidal Systems of a Substance in the Form of Nanoparticles. U.S. Patent 5,049,322, 1991.
(35) Koppel, D. E. Analysis of Macromolecular Polydispersity in Intensity Correlation Spectroscopy: The Method of Cumulants. *J. Chem. Phys.* **1972**, *57*, 4814−4820.
(36) Brader, J. M.; Siebenbürger, M.; Ballauff, M.; Reinheimer, K.; Wilhelm, M.; Frey, S. J.; Weysser, F.; Fuchs, M. Nonlinear Response of Dense Colloidal Suspensions Under Oscillatory Shear: Mode-Coupling Theory and Fourier Transform Rheology Experiments. *Phys. Rev. E: Stat., Nonlinear, Soft Matter Phys.* **2010**, *82*, 61401.
(37) Srivastava, S.; Shin, J. H.; Archer, L. A. Structure and Rheology of Nanoparticle-Polymer Suspensions. *Soft Matter* **2012**, *8*, 4097−4108.
(38) Koumakis, N.; Pamvouxoglou, A.; Poulos, A. S.; Petekidis, G. Direct Comparison of the Rheology of Model Hard and Soft Particle Glasses. *Soft Matter* **2012**, *8*, 4271−4284.
(39) Carrier, V.; Petekidis, G. Nonlinear Rheology of Colloidal Glasses of Soft Thermosensitive Microgel Particles. *J. Rheol.* **2009**, *53*, 245−273.
(40) Laurati, M.; Egelhaaf, S. U.; Petekidis, G. Non-linear Rheology of Colloidal Gels with Intermediate Volume Fraction. *J. Rheol.* **2011**, *55*, 673.
(41) Di Giuseppe, E.; Davaille, A.; Mittelstaedt, E.; François, M. Rheological and Mechanical Properties of Silica Colloids: From Newtonian Liquid to Brittle Behaviour. *Rheol. Acta* **2012**, *51*, 1−15.
(42) Arunan, E.; Desiraju, G. R.; Klein, R. A.; Sadlej, J.; Scheiner, S.; Alkorta, I.; Clary, D. C.; Crabtree, R. H.; Dannenberg, J. J.; Hobza, P.; Kjaergaard, H. G.; Legon, A. C.; Mennucci, B.; Nesbitt, D. J. Defining the Hydrogen Bond: An Account (IUPAC Technical Report). *Pure Appl. Chem.* **2011**, *83*, 1619−1636.
(43) Rinaudo, M. Non-covalent Interactions in Polysaccharide Systems. *Macromol. Biosci.* **2006**, *6*, 590−610.
(44) Sorlier, P.; Denuziere, A.; Viton, C.; Domard, A. Relation between the Degree of Acetylation and the Electrostatic Properties of Chitin and Chitosan. *Biomacromolecules* **2001**, *2*, 765−772.
(45) Omelczuk, M. O.; McGinity, J. W. The Influence of Polymer Glass Transition Temperature and Molecular Weight on Drug Release from Tablets Containing Poly(DL-lactic acid). *Pharm. Res.* **1992**, *9*, 26−32.
(46) Passerini, N.; Craig, D. Q. M. An Investigation into the Effects of Residual Water on the Glass Transition Temperature of Polylactide Microspheres Using Modulated Temperature DSC. *J. Controlled Release* **2001**, *73*, 111−115.
(47) Messai, I.; Lamalle, D.; Munier, S.; Verrier, B.; Ataman-Önal, Y.; Delair, T. Poly(d,l-lactic Acid) and Chitosan Complexes: Interactions with Plasmid DNA. *Colloids Surf., A* **2005**, *255*, 65−72.
(48) Walker, H. W.; Grant, S. B. Influence of Surface Charge and Particle Size on the Stabilization of Colloidal Particles by Model Polyelectrolytes. *Colloids Surf., A* **1998**, *135*, 123−133.

(49) Tsaih, M. L.; Chen, R. H. Effect of Molecular Weight and Urea on the Conformation of Chitosan Molecules in Dilute Solutions. *Int. J. Biol. Macromol.* **1997**, *20*, 233−240.
(50) Guo, C.; Gemeinhart, R. A. Understanding the Adsorption Mechanism of Chitosan onto Poly(lactide-co-glycolide) Particles. *Eur. J. Pharm. Biopharm.* **2008**, *70*, 597−604.
(51) Hanus, L. H.; Ploehn, H. J. Conversion of Intensity-Averaged Photon Correlation Spectroscopy Measurements to Number-Averaged Particle Size Distributions. 1. Theoretical Development. *Langmuir* **1999**, *15*, 3091−3100.
(52) Popa-Nita, S.; Rochas, C.; David, L.; Domard, A. Structure of Natural Polyelectrolyte Solutions: Role of the Hydrophilic/Hydrophobic Interaction Balance. *Langmuir* **2009**, *25*, 6460−6468.
(53) Glatter, O.; Kratky, O. *Small Angle X-ray Scattering*; Academic Press: New York, 1982.
(54) Berth, G.; Dautzenberg, H. The Degree of Acetylation of Chitosans and Its Effect on the Chain Conformation in Aqueous Solution. *Carbohydr. Polym.* **2002**, *47*, 39−51.
(55) Kona, S.; Specht, D.; Rahimi, M.; Shah, B. P.; Gilbertson, T. A.; Nguyen, K. T. Targeted Biodegradable Nanoparticles for Drug Delivery to Smooth Muscle Cells. *J. Nanosci. Nanotechnol.* **2012**, *12*, 236−244.